HHS Public Access

Author manuscript

Cell Stem Cell. Author manuscript; available in PMC 2019 January 04.

Published in final edited form as:

Cell Stem Cell. 2018 January 04; 22(1): 119–127.e3. doi:10.1016/j.stem.2017.11.009.

Muscle stem cells exhibit distinct clonal dynamics in response to tissue repair and homeostatic aging

Matthew T Tierney[1,2,3], **Michael J Stec**[2], **Steffen Rulands**[4,5], **Benjamin D Simons**[4], and **Alessandra Sacco**[2]

[1]Graduate School of Biomedical Sciences, Sanford Burnham Prebys Medical Discovery Institute, 10901 N Torrey Pines Road, La Jolla, CA 92037

[2]Development, Aging and Regeneration Program, Sanford Burnham Prebys Medical Discovery Institute, 10901 N Torrey Pines Rd, La Jolla, CA 92037 USA

[4]Cavendish Laboratory, Department of Physics, J. J. Thomson Avenue, Cambridge CB3 0HE, UK; The Wellcome Trust/Cancer Research UK Gurdon Institute, University of Cambridge, Tennis Court Road, Cambridge CB2 1QN, UK; Wellcome Trust-Medical Research Council Stem Cell Institute, University of Cambridge, UK

Summary

Clonal complexity of adult stem cell pools is progressively lost during homeostatic turnover in several tissues, suggesting a decrease in the number of stem cells with distinct clonal origins. The functional impact of reduced complexity on stem cell pools, and how different tissue microenvironments may contribute to such a reduction, is poorly understood. Here we performed clonal multicolor lineage tracing of skeletal muscle stem cells (MuSCs) to address these questions. We found that MuSC clonal complexity is maintained during aging despite heterogenous reductions in proliferative capacity, allowing aged muscle to mount a clonally diverse, albeit diminished, response to injury. In contrast, repeated bouts of tissue repair cause a progressive reduction in MuSC clonal complexity indicative of neutral drift. Consistently, biostatistical modeling suggests MuSCs undergo symmetric expansions with stochastic fate acquisition during tissue repair. These findings establish distinct principles that underlie stem cell dynamics during homeostatic aging and repeated muscle regeneration.

Lead contact and Corresponding author: Alessandra Sacco, Ph.D., Development, Aging and Regeneration Program, Sanford Children's Health Research Center, Sanford Burnham Prebys Medical Discovery Institute, 10901 North Torrey Pines Road, La Jolla, CA 92037, USA, Tel: 858-597-5337, asacco@sbpdiscovery.org.

[3]Current affiliation: Robin Chemers Neustein Laboratory of Mammalian Cell Biology and Development, Howard Hughes Medical Institute, The Rockefeller University, New York, NY 10065 USA

[5]Current affiliation: Max Planck Institute for the Physics of Complex Systems, Noethnitzer Str. 38, 01187 Dresden Germany; Center for Systems Biology Dresden, Pfotenhauer Str. 108, 01307 Dresden, Germany

Author Contributions: Conceptualization, M.T.T. and A.S.; Methodology, M.T.T., S.R., B.D.S. and A.S.; Validation, M.J.S.; Formal Analysis, S.R. and B.D.S.; Investigation, M.T.T., M.J.S.; Writing – Original Draft, M.T.T. and A.S.; Writing – Review & Editing, M.T.T., M.J.S. S.R., B.D.S. and A.S.; Visualization, M.T.T. and A.S.; Supervision, B.D.S. and A.S.; Project Administration, B.D.S. and A.S.; Funding Acquisition, A.S.

Graphical abstract

Tierney et al. use multicolor lineage tracing at clonal levels to demonstrate the control of muscle stem cell asymmetry is context-dependent, coordinated by individual divisions with homeostatic turnover and at the population level during tissue repair.

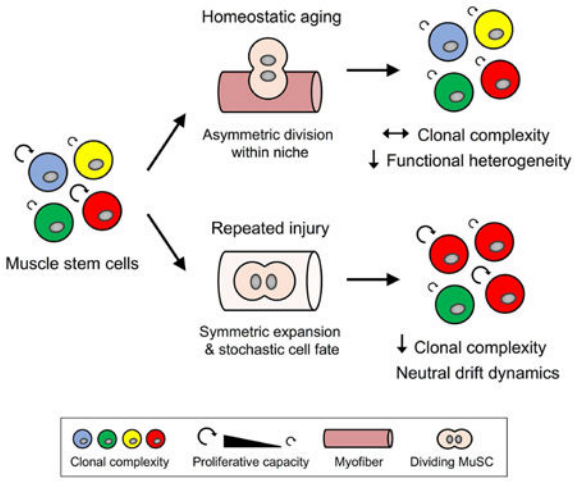

Keywords

Stem cells; skeletal muscle; functional heterogeneity; clonal complexity; homeostasis; aging; regeneration; multicolor lineage tracing; clonal behavior; biostatistical modeling

Introduction

Emerging evidence supports a significant functional heterogeneity in adult stem cell compartments. Single cell studies in several tissues have revealed a range of behavioral capacities with regard to proliferation, self-renewal, and differentiation potential (Krieger and Simons, 2015). This heterogeneity has been proposed as a beneficial feature of stem cells, which must rapidly adjust to the changing demands of their host tissue. By maintaining a spectrum of functional abilities, stem cells are better prepared to respond to various tissue repair scenarios while contributing to homeostatic turnover.

Single cell lineage tracing offers a powerful means of studying functional heterogeneity in stem cells. Prior lineage tracing studies *in vivo* have demonstrated a broad array of clonal histories in different tissues (Bonaguidi et al., 2011; Doupe et al., 2010; Henninger et al., 2017). Modeling efforts leveraging these clonal data sets have begun to describe the dynamics of stem cell hierarchies (Blanpain and Simons, 2013; Klein and Simons, 2011). Intriguingly, several groups have described a loss of clonal complexity, or the diversity of stem cells in a pool or niche with distinct clonal origin, with accumulated stem cell activity (Klein et al., 2010; Nguyen et al., 2017; Snippert et al., 2010). However, much of this work has taken place during youthful tissue homeostasis and thus, little is known about how different environmental settings may alter the rate of this decline over time, including aging or wound healing. Moreover, the impact that reductions in clonal complexity may have on

functional heterogeneity and stem cell behavior is still unclear. To answer these questions, it is critical to study both aspects of individual stem cell behavior as part of the greater whole, particularly within a readily manipulated host tissue.

To this end, skeletal muscle is well-suited to examine changes in stem cell heterogeneity in response to disruptive or pathological settings. Skeletal muscle contains a bona fide stem cell population, termed muscle stem cells (MuSCs) or satellite cells, distributed throughout the tissue in their niche where they remain poised to activate and contribute to cellular turnover (Brack and Rando, 2012). MuSCs support tissue homeostasis and are an indispensable part of the repair process, directly contributing to myonuclear accretion in both contexts (Yin et al., 2013).

MuSCs are functionally heterogeneous as subsets with distinct long-term stem cell potential have been identified on the basis of *Pax7* and *Myf5* levels, two key transcription factors involved in the determination of MuSC fate (Kuang et al., 2007; Rocheteau et al., 2012). Intrinsic failures combined with microenvironmental and systemic alterations collectively decrease MuSC number and self-renewal potential with age (Chakkalakal et al., 2012; Cosgrove et al., 2014; Lukjanenko et al., 2016; Sousa-Victor et al., 2014; Tierney et al., 2014). Changes in the rates of asymmetric and symmetric divisions have implicated imbalances in functional heterogeneity as underlying factors contributing to these inefficiencies (Bernet et al., 2014; Price et al., 2014). Conversely, MuSC-mediated regeneration is scarless with complete restoration of tissue function and efficient repopulation of the stem cell pool. Potential changes in functional heterogeneity or clonal complexity in either setting, however, remain largely unexplored.

To determine the impact of homeostatic aging and tissue repair on MuSC clonal complexity, we longitudinally assessed individual MuSC fate over time using *in vivo* multicolor lineage tracing. Surprisingly, we demonstrated that clonal complexity is largely preserved with homeostatic aging despite reductions in proliferative heterogeneity. Conversely, biostatistical modeling revealed that MuSCs undergo symmetric expansion and stochastic cell fate acquisition specifically during tissue repair, predicting neutral competition between clones resulting in clonal drift, or an increasingly small number of dominant clones. Accordingly, we observed that sustained regenerative pressure resulted in a progressive reduction in clonal complexity. Overall, this work establishes the importance of context in defining the principles underlying stem cell dynamics in skeletal muscle.

Results

Polyclonal contribution of MuSCs to skeletal muscle homeostasis with age

To enable clonal fate mapping in MuSCs, we generated *Pax7-CreER™;R26R*$^{Brainbow2.1}$ mice by crossing the *R26R*$^{Brainbow2.1}$ reporter (Snippert et al., 2010) with a *Pax7-CreER™* driver (Nishijo et al., 2009). Here, Pax7 inducibly drives expression of the *Brainbow-2.1* multicolor reporter specifically in MuSCs (Figure S1A). Tamoxifen (tmx) administration at postnatal days 24-28, immediately prior to the establishment of the adult MuSC pool (Chakkalakal et al., 2014; Tierney et al., 2016), resulted in the stochastic labeling of Pax7^{+} MuSCs with one of four fluorescent proteins (FPs): membrane-bound cyan (CFP), nuclear

green (GFP), cytoplasmic yellow (YFP), or cytoplasmic red (RFP) (Figure S1B). Labeled mice were maintained for either 2-3 months (young) or 24-26 months (aged) prior to harvest (Figure 1A). MuSC labeling frequency was stable over time, measured on single isolated myofibers as 51.0 ± 3.1% in young muscles and maintained (52.4 ± 2.9%) with age (Figure S1C). Although the cyan, yellow and red FPs appeared at near-equivalent ratios, GFP^+ MuSCs were found less frequently than expected from random rates of excision or inversion, as previously reported (Snippert et al., 2010) (Figure S1D).

We first set out to determine the diversity of MuSC contribution to homeostatic maintenance over time. Prior efforts have demonstrated a significant accumulation of MuSC fusion to myofibers with age absent injury (Keefe et al., 2015; Pawlikowski et al., 2015). However, the degree to which all MuSCs participate in this process has not been studied. Thus, we measured the contribution of each FP from labeled MuSCs to myofibers with age (Figure 1A). Aged mice predictably exhibited signs of sarcopenia when measuring myofiber cross-sectional area (CSA) in tibialis anterior (TA) muscles (Figure 1B-C). We detected a widespread contribution of labeled MuSCs to aged muscles (Figure 1D). The frequency of expression across FPs was comparable and consistent with measurements on single myofiber-associated MuSCs, as only GFP^+ nuclei were detected more rarely (Figure S1E). Notably, 52.7 ± 6.3% of aged myofibers were polyclonal, expressing at least two FPs (Figure 1D). When considering the submaximal recombination efficiency of MuSCs in these muscles, this result indicates that myonuclear turnover with age *in vivo* is the responsibility of several MuSCs associated with each myofiber.

Loss of functional heterogeneity, but not clonal complexity, in MuSCs with age

Potential losses in clonal complexity or functional heterogeneity with age can be achieved by changes in division dynamics or stem cell depletion, both established features of aged MuSCs (Bernet et al., 2014; Sousa-Victor et al., 2014). To determine whether aged MuSCs maintain youthful levels of either measure over time, we examined the composition of single myofiber-associated MuSCs (Figure 2A).

Because MuSCs are thought to be retained on their native myofiber under homeostatic conditions (Webster et al., 2015), changes in clonal complexity might be more readily observed in this compartment. The number of $Pax7^+$ MuSCs associated with freshly isolated single myofibers was reduced with age (Figure S2A). However, we did not observe changes in the local distribution of labeled MuSCs of each color within individual young and aged single myofibers, suggesting that aged muscles may maintain a clonally complex assortment of MuSCs (Figure S2B). For functional assessment, single myofibers and their associated MuSCs were cultured in suspension under growth conditions for 3 days. Spatially separated FP^+ MuSC clones were frequently observed (Figure 2B). Their faithful identification was confirmed by a low frequency of clonal merging events (overlapping MuSC clones labeled with different FPs, 1.6 ± 1.4%) (Figure S2C). Aged MuSC clone size was smaller overall, confirming previous reports of impaired proliferative potential (Cosgrove et al., 2014; Sousa-Victor et al., 2014) (Figure 2C). Myofiber-associated MuSCs asynchronously undergo spontaneous differentiation in culture, with only a subset retaining a stem cell profile marked by Pax7 expression. Although we observed heterogeneity regardless of age, there was no

difference in the overall levels of Pax7 expression between young and aged MuSCs (Figure 2C).

In vivo examination of MuSC clonal complexity with age similarly requires their activation for assessment, accomplished by inducing a regenerative event. Thus, we performed barium chloride ($BaCl_2$) injury in extensor digitorum longus (EDL) muscles of tmx-treated young and aged mice. Sectioning along its longitudinal axis revealed labeled MuSC progeny as a mosaic of clonal units within degraded myofibers during the peak proliferative phase 3 days post-injury. While mean clone size was again smaller in aged muscles, we did not find differences in the rate of early myogenic differentiation as measured by Myod expression (Figure 2D-E). Although clonal merging rates were slightly higher than the rates observed *ex vivo* (4.9 ± 2.3%), we refined our data set by filtering for veritable clones on the basis of our observed merging rate (Supplementary Methods). Confirmation of clonal identity was further demonstrated by a tight overlap between the size distributions of multicolor and GFP^+ clones, a minority color whose probability of merging is especially low (Figure S2D-E). Importantly, the variance of aged MuSC clone size was significantly reduced *in vivo*, indicating reduced proliferative heterogeneity (Figure 2E). The Gini coefficient, a statistical measure of dispersion, was also decreased in clone size distributions with age (0.306 and 0.261 in young and aged samples, respectively; a value of 0 indicates complete homogeneity while a value of 1 indicates maximal heterogeneity) (Jiang et al., 2016). Thus, functional MuSC heterogeneity is reduced with age.

Examination of regenerating muscles was performed after the conclusion of muscle repair at 25 days after $BaCl_2$ injury (Figure 2F-G). The nucleus of donor MuSCs adopts a central position within the myofiber once fused, distinguishing newly repaired from undamaged skeletal muscle. Regenerated myofiber cross-sectional area (CSA) was smaller in aged muscles, in agreement with decreased MuSC number and proliferative potential (Figure 2H). However, aged myofibers contained a full assortment of FPs following regeneration, showing no differences in labeled FP distribution per myofiber or detection frequency for each FP between young and aged muscles (Figures 2G, 2I and S2F). These findings support the unanticipated view that although functional heterogeneity is decreased, clonal complexity is conserved with age. Consequently, aged MuSCs remain able to mount a balanced regenerative response on the basis of clonal origin.

Aged MuSCs maintain adherence to a model of symmetric expansion and stochastic cell fate acquisition during tissue repair

To understand the paradigms underlying MuSC regenerative behavior, including whether or not they become altered with age, we performed biostatistical modeling with our *in vivo* clonal data sets. To properly constrain our model, we made use of published data from single myofiber cultures measuring the onset of MuSC division and proliferative rate following activation (Siegel et al., 2011). Cell cycle length after the first and second divisions was uncorrelated and independent of the onset of proliferation, suggesting that proliferation may be stochastic (Figure S3A). When applied to our clone size distributions 3 days post-injury, this information allowed us to increase predictive power and better describe MuSC dynamics during regeneration.

Both young and aged MuSC behavior could be most accurately captured quantitatively by the same model of exponential growth driven by symmetric division, further indicating that age-associated functional decline is not accompanied by compositional changes to the population at large (Figure 3A-B, Supplementary Methods). Impaired expansion of aged MuSCs was confirmed by inferred division rates of 1.2 and 1.0 per day in young and aged MuSCs, respectively. Thus, the overall mode of MuSC regenerative behavior was unaltered following acute injury, in spite of their reduced proliferative capacity.

Intriguingly, the best-fit model also predicted that young and aged stem cell fate during tissue repair is specified randomly with each cell division (Figure 3A-B). This quality, including symmetric expansion, is supported by recent intravital imaging experiments demonstrating that MuSCs primarily undergo longitudinally-oriented planar divisions within damaged myofibers (Webster et al., 2015). Stochastic cell fate acquisition has been strongly associated with progressive reductions in clonal complexity within several adult stem cell pools (Blanpain and Simons, 2013). Although we did not observe this with age, stem cell activity under homeostatic conditions takes place in an environmental setting that is fundamentally different from tissue damage and repair. Therefore, this finding suggests that clonal complexity in the MuSC pool might be differentially affected by wound healing, as opposed to normal homeostatic turnover.

Progressive clonal drift in MuSCs with repeated bouts of regeneration

To assess the potentially distinct effects of sustained regenerative pressure on MuSC clonal complexity, we performed repeated bouts of $BaCl_2$ injury in young muscles (Figure 3C-D). No differences in myofiber CSA were measured after each successive injury, evidence that 25 day intervals were adequate to complete a full regenerative cycle (Figure 3E). However, the distribution of FP^+ myofibers across muscles shifted with successive injuries, characterized by increasingly visible FP clustering and segregation. A greater percentage of myofibers in serially injured muscles contained only one FP while significantly fewer myofibers contained two or more FPs, suggesting a decrease in MuSC clonal complexity with accumulated regenerative activity (Figure 3F). This occurred despite no changes in the relative ratio of myofibers expressing each FP over the full injury series, indicating that this result was due to regional changes in FP composition and not to a reduction in the overall percentage of FP^+ myofibers (Figure S3B).

In addition to predicting a loss of clonal complexity, our model of regenerative MuSC behavior (Figure 3B) supports a theoretical framework of population asymmetry. Here, the stem cell pool is maintained through competitively balanced clonal extinction and compensatory expansion of neighboring clones, leading to clonal drift (Blanpain and Simons, 2013). Alternatively, a competing model of invariant asymmetry proposes that individual stem cell divisions are predominately asymmetric to allow for the enduring self-renewal of a stem cell subset. Invariant asymmetry is thought to be more likely in a highly polarized and well-defined microenvironment, features of the MuSC niche under homeostatic conditions but rapidly lost as the niche becomes disrupted with injury (Yin et al., 2013). To distinguish between these models of MuSC behavior during tissue repair, we measured patterning by taking advantage of the low labeling frequency and nuclear

localization of GFP. We could identify GFP^+ clusters of regenerating myofibers in tissue cross-sections, defined as adjacent myofibers containing GFP^+ MuSC-derived central nuclei (Figure 4A). A mosaic of GFP^+ myofiber clusters stable in size and number would support a model of invariant asymmetry. Instead, population asymmetry would be corroborated by a progressive increase in average MuSC cluster size over time and a reduction in the total number of clusters.

Consistently, the population asymmetry model was upheld in this scenario, as we observed a progressive reduction in myofiber cluster density together with an increase in the average number of GFP^+ myofibers within each cluster (Figure 4B-C). The total number of GFP^+ myofibers per unit area was maintained, ruling out the possibility that reductions in labeling frequency are responsible for this effect (Figure S4A). Despite changes in cluster size and number, curves generated from normalized cluster size distributions after successive injuries overlapped with each other. This is a hallmark of scaling behavior theorized by population asymmetry and consistent with clonal drift due to neutral competition between MuSCs (Figure 4D). Indeed, curve fitting of the scaling function suggested that the fate of each MuSC is acquired randomly during skeletal muscle repair (Klein and Simons, 2011). Scaling behavior predicts that MuSC clone loss and compensatory expansion occur with equal probability as clone size grows linearly, consistent with our clone size measurements. Therefore, reductions in clonal complexity through stem cell replacement characterizes MuSC behavior under prolonged tissue repair.

Finally, an index based upon nearest neighbor distances between GFP^+ nuclei confirmed a gradual increase in GFP^+ myofiber clustering in serially injured muscles, despite unchanged overall concentrations of GFP^+ nuclei (Figures 4E, S4B, Supplementary Methods). Plotting the cumulative distribution frequency of GFP^+ nuclei showed a similar trend (Figure 4F). The distribution of GFP^+ MuSCs in all groups showed patterns that departed significantly from a Poisson, or random, process, consistent with low MuSC labeling efficiencies necessary for clonal approximations. The total distance interval distributions also increasingly deviate from a Gaussian function with serial injuries, further establishing spatial clustering as a feature of MuSCs over multiple regenerative events (Figure S4C). By comparison, we observed no change in GFP^+ myofiber cluster size or density or these spatial patterning metrics in young and aged muscles after a single injury, distinguishing homeostatic aging from regeneration as it relates to the coordination of population-level stem cell activity (Figure S4D-G). Collectively, these findings show that MuSCs follow a model of population asymmetry and undergo progressive clonal drift selectively under constant regenerative pressure.

Discussion

A tightly controlled balance between self-renewal and differentiation is necessary to preserve the precise number of stem cells needed in support of healthy tissue function. Here, we performed multicolor lineage tracing at clonal levels to dynamically assess young and aged MuSC fate *in vivo*. We demonstrated that MuSC clonal complexity is largely preserved with age under homeostatic conditions, despite declines in proliferative heterogeneity. Conversely, clonal drift and consequent reduction of clonal complexity was observed with

successive injuries. Thus, MuSC asymmetry is coordinated at the population level uniquely under sustained regenerative pressure while homeostatic turnover instead manages this asymmetry at the level of individual cell divisions, defining the distinct principles underlying stem cell dynamics in skeletal muscle with age and tissue repair.

Work in several high-turnover stem cell compartments has often, but not exclusively, endorsed a model of population asymmetry under homeostatic conditions. For example, while resident epidermal stem cells balance asymmetric cell fate through neutral competition during homeostatic maintenance (Mascre et al., 2012), wound healing instead recruits stem cells from distinct epidermal regions that exhibit hierarchical behavior, either dividing asymmetrically or undergoing one round of symmetric division during the expansion phase to then yield progenitors that follow stochastic cell fate acquisition (Aragona et al., 2017). In regenerating skeletal muscle, we find that stochastic stem cell loss is compensated by the expansion of neighboring clones, leading to neutral drift dynamics. We cannot rule out that MuSCs do not follow this behavioral pattern during normal aging because of insufficient turnover, as they divide more slowly under homeostatic conditions. However, a substantial accumulation of activity over the large majority of the mouse lifespan is evidenced by the diverse contribution of MuSC progeny to aged myofibers, suggesting that proliferative activity alone may not account for this deviation from cell fate behavior.

Differences in microenvironmental factors between homeostatic and regenerative conditions also likely contribute to our observed differences in the maintenance of clonal complexity. Uninjured muscles preserve MuSCs in a highly polarized niche that is amenable to repeated asymmetric division. These features likely support behavior that is consistent with a model of invariant asymmetry, in which clonal complexity is more likely to persist over time. On the other hand, injury disrupts this niche and demands that MuSCs replace lost myonuclei by undergoing serial rounds of symmetric division within the void left by degraded myofibers (Gurevich et al., 2016; Webster et al., 2015). Lost polarization, non-uniform contact with the neighboring matrix, support cell types and exposure to varied soluble cues all constitute a less well-defined microenvironment that may favor stochastic cell fate acquisition. The integration of rapid, symmetric stem cell expansion with neutral competition to later generate differentiated progeny is well aligned with optimality theory in adult stem cells during morphogenesis, when the niche is still being defined (Itzkovitz et al., 2012). A less structured niche prior to its full establishment is also characteristic of skeletal muscle during early development, where MuSC precursors have recently been shown to undergo neutral drift dynamics in zebrafish (Nguyen et al., 2017). Thus, environmental setting may contribute to the facultative use of different division modes to balance the ultimate number of MuSCs and the differentiated progeny.

It remains possible that tissue homeostasis and regeneration are managed by separate cellular subsets that have different propensities for either model of stem cell behavior. Pulse-chase studies have described heterogeneity in aged MuSC regenerative capacity on the basis of label retention (Chakkalakal et al., 2012). MuSCs atop the stem cell hierarchy may represent a reserve pool, opting to preserve their self-renewal potential while relying on progenitors for the bulk of tissue homeostasis as in the hematopoietic system (Sun et al., 2014). Lineage tracing of label-retaining cells in the intestinal crypt has suggested that they

contribute only after injury (Buczacki et al., 2013). If true in skeletal muscle, the selective engagement of reserve MuSCs during regeneration may be sufficient to modify collective behavioral patterns. Furthermore, communication between stem cell subsets reinforce cellular identity and help determine fate choices in support of niche integrity and tissue function (Hsu et al., 2014; Ouspenskaia et al., 2016). Differential activity in these subsets may similarly alter these interactions and impact MuSC behavioral models.

Finally, young MuSCs were able to efficiently regenerate muscle with serial injury despite reductions in clonal complexity, calling into question the potential consequences of this model. Although population asymmetry allows for neighboring MuSCs to compensate for clones that succumb to selective pressures, they then acquire a disproportionate share of the total pool. Advancement towards clonal collapse, either through disparate environmental interactions or acquired genomic mutation, is associated with age-related adverse health outcomes in the blood and skin, including tumorigenesis (Jaiswal et al., 2014; Martincorena et al., 2015). Therefore, a chronic regenerative response may continue to exacerbate stem cell imbalance and ultimately lead to deleterious outcomes, providing a therapeutic rationale for strategies designed to maintain clonal complexity.

In conclusion, this work demonstrates that clonal complexity in the MuSC pool is preserved with age but progressively depleted with repeated bouts of tissue repair, supporting a model of population asymmetry and clonal drift specifically in regenerating skeletal muscle. These findings may have implications for chronic muscle degenerative diseases, where unrelenting regenerative pressure may lead to reductions in MuSC clonal complexity that ultimately contribute to tissue dysfunction. Finally, this work demonstrates the importance of considering cell behavior both individually and as a collective whole, providing insight into the central processes that regulate stem cell function, heterogeneity, and regenerative potential.

Star Methods

Contact for Reagent and Resource Sharing

Further information and requests for resources and reagents should be directed to and will be fulfilled by the Lead Contact, Alessandra Sacco, Ph.D. (asacco@sbpdiscovery.org).

Experimental Model and Subject Details

Animals

All animal protocols were approved by the Sanford Burnham Prebys Medical Discovery Institute (SBPMDI) Animal Care Committees. Mice were housed according to institutional guidelines, in a controlled environment at a temperature of 22C+/-1C, with 12/12 hr light/dark cycles and diet and water ad libitum. *Pax7CreER™* mice, a kind gift from C. Keller (Nishijo et al., 2009), and *R26R*$^{Brainbow2.1}$ (Snippert et al., 2010) mice, purchased from Jackson Laboratories, were used to generate *Pax7-CreER™;*R26R$^{Brainbow2.1}$ mice. Both male and female mice were used, heterozygous for both *Pax7-CreER™* and *R26R*$^{Brainbow2.1}$ alleles, bred in-house, and maintained on a C57BL/6J background. All the subjects were not involved in any previous procedures.

Methods Details

Animal procedures

Tamoxifen (tmx) was resuspended in corn oil at 20 mg ml^{-1} and administered daily at 100 mg kg^{-1} body weight via intraperitoneal (i.p.) injection at postnatal days 24-28 (P24-28). Prior to skeletal muscle injury, mice were anesthetized by 1-4% L min^{-1} O_2 isofluorane inhalation. The tibialis anterior (TA) and extensor digitorum longus (EDL) muscles were "stabbed" 10 times before injecting 50 μl barium chloride suspended in PBS (1.2% w/v, Sigma) in several locations to evenly distribute the solution throughout both muscles.

Single myofiber isolation and culture

Single myofibers were prepared as previously described (Sacco et al., 2010). The gastrocnemius (GAS) muscles were harvested and subjected to enzymatic dissociation (700 units ml^{-1} type II collagenase, Life Technologies) for 60 min at 37 °C. Dissociated single myofibers were manually collected and purified under a dissection microscope, then either fixed immediately in 1.5% paraformaldehyde (PFA) for 15 min or maintained in suspension culture for 72 h with growth media (GM) composed of Dulbecco's Modified Eagle's Medium (DMEM) containing 1 g L^{-1} D-glucose, L-glutamine and 110 mg L^{-1} sodium pyruvate and 10% horse serum (HS) for 48 h, then adding 15% fetal bovine serum (FBS) for the remaining 24 h before fixation.

Immunofluorescence

Muscle tissues were prepared for histology as previously described (Sacco et al., 2005). The TA and EDL muscles were fixed in 0.5% PFA for 4 h at 4 °C, treated in 20% w/v sucrose overnight, frozen and stored at -80 °C unti l cryosectioning. Myofiber-associated satellite cells (SCs) and muscle sections were permeabilized in 0.1% Triton and blocked in 20% goat serum. Incubation with the primary antibodies was performed overnight at 4 °C. The antibodies used were: mouse anti-Pax7 (1:100, DSHB), mouse anti-Myod (1:100, Santa Cruz), rabbit anti-laminin (1:200, Sigma), and Alexa-conjugated secondary antibodies (1:400, Invitrogen). Images were acquired using a LSM170 laser-scanning confocal microscope, 20X/0.8 Plan-Apochromat or 40X/1.3 Plan NeoFluar oil objectives and ZEN 2011 imaging software (Zeiss) or a Leica DMi8 confocal microscope and TCS SP8 laser scanning platform, 10X/0.3 HC PL Fluotar, 20X/0.75 HC PL APO IMM CORR CS2 or 40X/1.3 HC PL APO OIL CS2 objectives and LAS X imaging software (Leica). All composite images were stitched together and prepared in ZEN 2011 imaging software (Zeiss) using the Tiles module. Because imaging strategies for cytoplasmic YFP were not able to filter and remove nuclear GFP fluorescence in muscle cross-sections, their unique cellular localization was leveraged to warrant subtraction of non-specific signal (ImageJ). Excluding this exception, all images were composed, edited and modifications applied to the whole image using Photoshop CS6 (Adobe).

Biostatistical modeling

When analyzing clonal data at early regenerative time points, we sought to define the simplest model that is capable of describing the measured clone size distributions. The

interpretation of the clonal data is complicated by the possibility of merging events between clones of equivalent color. To estimate the frequency of such unicolor mergers, we calculated the probability that a clone merges with a clone of a different color (denoted as bicolor mergers). If the induction frequency of the three majority colors is approximately equal then the probability of unicolor merging is approximately equal to the probability of bicolor merging (Aragona et al., 2017). With a frequency of bicolor merging of 4.9 ± 2.3% from >140 young and old clones, we found that these events are relatively rare. To obtain an unambiguous dataset, we further filtered for clonal events by considering the probability that a given cluster is a merger given the number of labeled cells it contains. This likelihood is proportional to the number of cells in this cluster, such that larger clusters are more likely to be the result of mergers than smaller clusters. We therefore considered clusters of labeled cells with a size smaller than the 0.95 quantile to be clonal.

Having filtered for clonal events, we sought to model the data. To increase predictive power, we developed a model based on both our static clonal data and the analysis of published time-lapse imaging data of single myofiber-associated MuSCs (Siegel et al., 2011). These experiments indicate that the onset of proliferation after injury is delayed and broadly distributed between cells. Further, the cell cycle times after the first divisions are uncorrelated and independent of the time of onset. This suggests that the subsequent degree of proliferation is stochastic. When considered with the conclusions of recent intravital imaging studies of skeletal muscle regeneration (Webster et al., 2015), we conjectured that in the initial phase after the onset of proliferation both daughter cells remain in cell cycle, i.e. divisions are symmetric.

To describe clonal dynamics we defined the time t_0 between wounding and the onset of proliferation in a given cell and its distribution between cells, $g(t_0)$. For a given labeled cell, after the exit from quiescence the stochastic time evolution of the clone size distribution, $f(n; t)$, follows a Master equation of the form:

$$\frac{d}{dt}f(n;t) = \lambda(n-1;t) - \lambda n f(n;t),$$

Where λ is the proliferation rate. If the clone consists at t_0 of a cells, the solution for $t > t_0$ follows a negative binomial form:

$$f(n;t) = \binom{n-1}{a-1} e^{-alt}\left(1-e^{-lt}\right)^{n-a},$$

Here, $a = 2$ for all clones. At the time of analysis, t_a, the clone size distribution is then obtained by ntegrating over all initiation times:

$$p(n;t) = \int_0^{t_a} (n, t_a - t_0) g(t_a) dt_0 .$$

To constrain possible model dynamics, we reasoned that the timing of exit from quiescence is similar n single myofiber suspension cultures and *in vivo*. We therefore fixed $g(t_0)$ by the empirical distribution of onset times found in (Siegel et al., 2011). This leaves the cell cycle rate, λ, as the only ree parameter of our model. We obtained λ by fitting $p(n; t)$ to the clonal data using maximum ikelihood estimation. We found that the most likely values were $\lambda = 0.026 \pm 0.003\ h^{-1}$ for young mice and $\lambda = 0.022 \pm 0.004\ h^{-1}$ for aged mice, corresponding to cell cycle rates of 39 hours and 46 hours, respectively.

Histological and spatial analyses

Quantification of fluorescence intensity in individual myofibers, measured as mean grey value, was performed with the masking strategy used for myofiber cross-sectional area quantification in an automated manner (Noirez et al., 2006) (ImageJ). Scoring of GFP-abeled MuSC patches was performed in stitched 2D mosaics encompassing the entire TA muscle (Leica). Euclidean total and nearest neighbor distances between GFP^+ nuclei were determined after conversion to binary images and point analysis to define their position within the muscle (ImageJ). The spatial distribution of GFP^+ nuclei was determined to be clustered (< 1.0), random (= 1.0) or egularly dispersed (1.1 – 2.5) by calculating a nearest neighbor index from nuclei-nuclei distance d, nuclei number n and nuclei density ρ using the following formula (Clark and Evans, 1954):

$$Nearest\ Neighbor\ Index = \frac{\sum d/n}{1/(2 \cdot \sqrt{\rho})}$$

Cumulative nearest neighbor distribution frequencies were plotted on survival curves and compared to a Poisson, or random, distribution using the following formula (Diggle, 1983):

$$f(x) = 1 - e^{(\rho \cdot \pi \cdot d^2)}$$

To distinguish between patterns of population asymmetric self-renewal, cluster size distributions were found to best fit the scaling function below:

$$f(x) = e^{-x}$$

Experimental Design

Preliminary experiments were performed when possible to determine requirements for sample size, taking into account resources available and ethical, reductionist animal use. Sample sizes were determined without formal power calculations. All animals were assigned to groups randomly, and investigators were not blinded to group allocation or outcome assessment. No samples or animals were excluded from this study. All attempts at replication were successful.

Quantification And Statistical Analysis

Data are presented as mean ± SEM unless otherwise indicated. Comparisons between samples following a Gaussian distribution used the student's t-test assuming two-tailed distributions with an alpha level of 0.05. Cumulative distributions of labeled, myofiber-associated MuSCs immediately after isolation were not assumed to be Gaussian; therefore, comparisons were performed using Kolmogorov-Smirnov test ($p < 0.05$). Comparisons between three or more samples were performed using one- or two-way ANOVA with Tukey's HSD test. Nearest neighbor distribution frequencies were compared to each other using the log-rank (Mantel-Cox) test or to a Poisson distribution using the Clark-Evans test (Clark and Evans, 1954). All statistical tests were performed using GraphPad Prism 6 for Macintosh.

Supplementary Material

Refer to Web version on PubMed Central for supplementary material.

Acknowledgments

We thank L. Boyd, B. Charbono, Amy Cortez and the Cell Imaging, Animal and Flow Cytometry Core Facilities at SBPMDI for technical support. We thank C. Keller for providing the *Pax7-CreER™* mice. We thank Dr. D Cornelison for her published data on MuSC division dynamics that were utilized for data modeling in this manuscript. This work was supported by the NIH R01 grant R01 AR064873 and SBPMDI start-up funds to A.S., and NIH grant F31 AR065923-03 to M.T.T.

References

Aragona M, Dekoninck S, Rulands S, Lenglez S, Mascre G, Simons BD, Blanpain C. Defining stem cell dynamics and migration during wound healing in mouse skin epidermis. Nat Commun. 2017; 8:14684. [PubMed: 28248284]

Bernet JD, Doles JD, Hall JK, Kelly Tanaka K, Carter TA, Olwin BB. p38 MAPK signaling underlies a cell-autonomous loss of stem cell self-renewal in skeletal muscle of aged mice. Nat Med. 2014; 20:265–271. [PubMed: 24531379]

Blanpain C, Simons BD. Unravelling stem cell dynamics by lineage tracing. Nat Rev Mol Cell Biol. 2013; 14:489–502. [PubMed: 23860235]

Bonaguidi MA, Wheeler MA, Shapiro JS, Stadel RP, Sun GJ, Ming GL, Song H. In vivo clonal analysis reveals self-renewing and multipotent adult neural stem cell characteristics. Cell. 2011; 145:1142–1155. [PubMed: 21664664]

Brack AS, Rando TA. Tissue-specific stem cells: lessons from the skeletal muscle satellite cell. Cell Stem Cell. 2012; 10:504–514. [PubMed: 22560074]

Buczacki SJ, Zecchini HI, Nicholson AM, Russell R, Vermeulen L, Kemp R, Winton DJ. Intestinal label-retaining cells are secretory precursors expressing Lgr5. Nature. 2013; 495:65–69. [PubMed: 23446353]

Chakkalakal JV, Christensen J, Xiang W, Tierney MT, Boscolo FS, Sacco A, Brack AS. Early forming label-retaining muscle stem cells require p27kip1 for maintenance of the primitive state. Development. 2014; 141:1649–1659. [PubMed: 24715455]

Chakkalakal JV, Jones KM, Basson MA, Brack AS. The aged niche disrupts muscle stem cell quiescence. Nature. 2012; 490:355–360. [PubMed: 23023126]

Clark PJ, Evans FC. Distance to Nearest Neighbor as a Measure of Spatial Relationships in Populations. Ecology. 1954; 35:445–453.

Cosgrove BD, Gilbert PM, Porpiglia E, Mourkioti F, Lee SP, Corbel SY, Llewellyn ME, Delp SL, Blau HM. Rejuvenation of the muscle stem cell population restores strength to injured aged muscles. Nat Med. 2014; 20:255–264. [PubMed: 24531378]

Diggle, P. Statistical analysis of spatial point patterns. London; New York: Academic Press; 1983.

Doupe DP, Klein AM, Simons BD, Jones PH. The ordered architecture of murine ear epidermis is maintained by progenitor cells with random fate. Dev Cell. 2010; 18:317–323. [PubMed: 20159601]

Gurevich DB, Nguyen PD, Siegel AL, Ehrlich OV, Sonntag C, Phan JM, Berger S, Ratnayake D, Hersey L, Berger J, et al. Asymmetric division of clonal muscle stem cells coordinates muscle regeneration in vivo. Science. 2016; 353:aad9969. [PubMed: 27198673]

Henninger J, Santoso B, Hans S, Durand E, Moore J, Mosimann C, Brand M, Traver D, Zon L. Clonal fate mapping quantifies the number of haematopoietic stem cells that arise during development. Nat Cell Biol. 2017; 19:17–27. [PubMed: 27870830]

Hsu YC, Li L, Fuchs E. Transit-amplifying cells orchestrate stem cell activity and tissue regeneration. Cell. 2014; 157:935–949. [PubMed: 24813615]

Itzkovitz S, Blat IC, Jacks T, Clevers H, van Oudenaarden A. Optimality in the development of intestinal crypts. Cell. 2012; 148:608–619. [PubMed: 22304925]

Jaiswal S, Fontanillas P, Flannick J, Manning A, Grauman PV, Mar BG, Lindsley RC, Mermel CH, Burtt N, Chavez A, et al. Age-related clonal hematopoiesis associated with adverse outcomes. N Engl J Med. 2014; 371:2488–2498. [PubMed: 25426837]

Jiang L, Chen H, Pinello L, Yuan GC. GiniClust: detecting rare cell types from single-cell gene expression data with Gini index. Genome Biol. 2016; 17:144. [PubMed: 27368803]

Keefe AC, Lawson JA, Flygare SD, Fox ZD, Colasanto MP, Mathew SJ, Yandell M, Kardon G. Muscle stem cells contribute to myofibres in sedentary adult mice. Nat Commun. 2015; 6:7087. [PubMed: 25971691]

Klein AM, Nakagawa T, Ichikawa R, Yoshida S, Simons BD. Mouse germ line stem cells undergo rapid and stochastic turnover. Cell Stem Cell. 2010; 7:214–224. [PubMed: 20682447]

Klein AM, Simons BD. Universal patterns of stem cell fate in cycling adult tissues. Development. 2011; 138:3103–3111. [PubMed: 21750026]

Krieger T, Simons BD. Dynamic stem cell heterogeneity. Development. 2015; 142:1396–1406. [PubMed: 25852198]

Kuang S, Kuroda K, Le Grand F, Rudnicki MA. Asymmetric self-renewal and commitment of satellite stem cells in muscle. Cell. 2007; 129:999–1010. [PubMed: 17540178]

Lukjanenko L, Jung MJ, Hegde N, Perruisseau-Carrier C, Migliavacca E, Rozo M, Karaz S, Jacot G, Schmidt M, Li L, et al. Loss of fibronectin from the aged stem cell niche affects the regenerative capacity of skeletal muscle in mice. Nat Med. 2016; 22:897–905. [PubMed: 27376579]

Martincorena I, Roshan A, Gerstung M, Ellis P, Van Loo P, McLaren S, Wedge DC, Fullam A, Alexandrov LB, Tubio JM, et al. Tumor evolution. High burden and pervasive positive selection of somatic mutations in normal human skin. Science. 2015; 348:880–886. [PubMed: 25999502]

Mascre G, Dekoninck S, Drogat B, Youssef KK, Brohee S, Sotiropoulou PA, Simons BD, Blanpain C. Distinct contribution of stem and progenitor cells to epidermal maintenance. Nature. 2012; 489:257–262. [PubMed: 22940863]

Nguyen PD, Gurevich DB, Sonntag C, Hersey L, Alaei S, Nim HT, Siegel A, Hall TE, Rossello FJ, Boyd SE, et al. Muscle Stem Cells Undergo Extensive Clonal Drift during Tissue Growth via Meox1-Mediated Induction of G2 Cell-Cycle Arrest. Cell Stem Cell. 2017; 21:107–119 e106. [PubMed: 28686860]

Nishijo K, Hosoyama T, Bjornson CR, Schaffer BS, Prajapati SI, Bahadur AN, Hansen MS, Blandford MC, McCleish AT, Rubin BP, et al. Biomarker system for studying muscle, stem cells, and cancer in vivo. FASEB J. 2009; 23:2681–2690. [PubMed: 19332644]

Noirez P, Torres S, Cebrian J, Agbulut O, Peltzer J, Butler-Browne G, Daegelen D, Martelly I, Keller A, Ferry A. TGF-beta1 favors the development of fast type identity during soleus muscle regeneration. J Muscle Res Cell Motil. 2006; 27:1–8. [PubMed: 16362724]

Ouspenskaia T, Matos I, Mertz AF, Fiore VF, Fuchs E. WNT-SHH Antagonism Specifies and Expands Stem Cells prior to Niche Formation. Cell. 2016; 164:156–169. [PubMed: 26771489]

Pawlikowski B, Pulliam C, Betta ND, Kardon G, Olwin BB. Pervasive satellite cell contribution to uninjured adult muscle fibers. Skelet Muscle. 2015; 5:42. [PubMed: 26668715]

Price FD, von Maltzahn J, Bentzinger CF, Dumont NA, Yin H, Chang NC, Wilson DH, Frenette J, Rudnicki MA. Inhibition of JAK-STAT signaling stimulates adult satellite cell function. Nat Med. 2014; 20:1174–1181. [PubMed: 25194569]

Rocheteau P, Gayraud-Morel B, Siegl-Cachedenier I, Blasco MA, Tajbakhsh S. A subpopulation of adult skeletal muscle stem cells retains all template DNA strands after cell division. Cell. 2012; 148:112–125. [PubMed: 22265406]

Sacco A, Doyonnas R, LaBarge MA, Hammer MM, Kraft P, Blau HM. IGF-I increases bone marrow contribution to adult skeletal muscle and enhances the fusion of myelomonocytic precursors. J Cell Biol. 2005; 171:483–492. [PubMed: 16275752]

Sacco A, Mourkioti F, Tran R, Choi J, Llewellyn M, Kraft P, Shkreli M, Delp S, Pomerantz JH, Artandi SE, et al. Short telomeres and stem cell exhaustion model Duchenne muscular dystrophy in mdx/mTR mice. Cell. 2010; 143:1059–1071. [PubMed: 21145579]

Siegel AL, Kuhlmann PK, Cornelison DD. Muscle satellite cell proliferation and association: new insights from myofiber time-lapse imaging. Skelet Muscle. 2011; 1:7. [PubMed: 21798086]

Snippert HJ, van der Flier LG, Sato T, van Es JH, van den Born M, Kroon-Veenboer C, Barker N, Klein AM, van Rheenen J, Simons BD, et al. Intestinal crypt homeostasis results from neutral competition between symmetrically dividing Lgr5 stem cells. Cell. 2010; 143:134–144. [PubMed: 20887898]

Sousa-Victor P, Gutarra S, Garcia-Prat L, Rodriguez-Ubreva J, Ortet L, Ruiz-Bonilla V, Jardi M, Ballestar E, Gonzalez S, Serrano AL, et al. Geriatric muscle stem cells switch reversible quiescence into senescence. Nature. 2014; 506:316–321. [PubMed: 24522534]

Sun J, Ramos A, Chapman B, Johnnidis JB, Le L, Ho YJ, Klein A, Hofmann O, Camargo FD. Clonal dynamics of native haematopoiesis. Nature. 2014; 514:322–327. [PubMed: 25296256]

Tierney MT, Aydogdu T, Sala D, Malecova B, Gatto S, Puri PL, Latella L, Sacco A. STAT3 signaling controls satellite cell expansion and skeletal muscle repair. Nat Med. 2014; 20:1182–1186. [PubMed: 25194572]

Tierney MT, Gromova A, Sesillo FB, Sala D, Spenle C, Orend G, Sacco A. Autonomous Extracellular Matrix Remodeling Controls a Progressive Adaptation in Muscle Stem Cell Regenerative Capacity during Development. Cell Rep. 2016; 14:1940–1952. [PubMed: 26904948]

Webster MT, Manor U, Lippincott-Schwartz J, Fan CM. Intravital Imaging Reveals Ghost Fibers as Architectural Units Guiding Myogenic Progenitors during Regeneration. Cell Stem Cell. 2015

Yin H, Price F, Rudnicki MA. Satellite cells and the muscle stem cell niche. Physiol Rev. 2013; 93:23–67. [PubMed: 23303905]

HIGHLIGHTS

- MuSC-mediated myonuclear turnover during homeostatic aging is polyclonal
- MuSCs show reduced functional heterogeneity but maintain clonal complexity with age
- Aged MuSCs retain behavioral patterns of population asymmetry during tissue repair
- MuSC exhibit a progressive reduction in clonal complexity following repeated injury

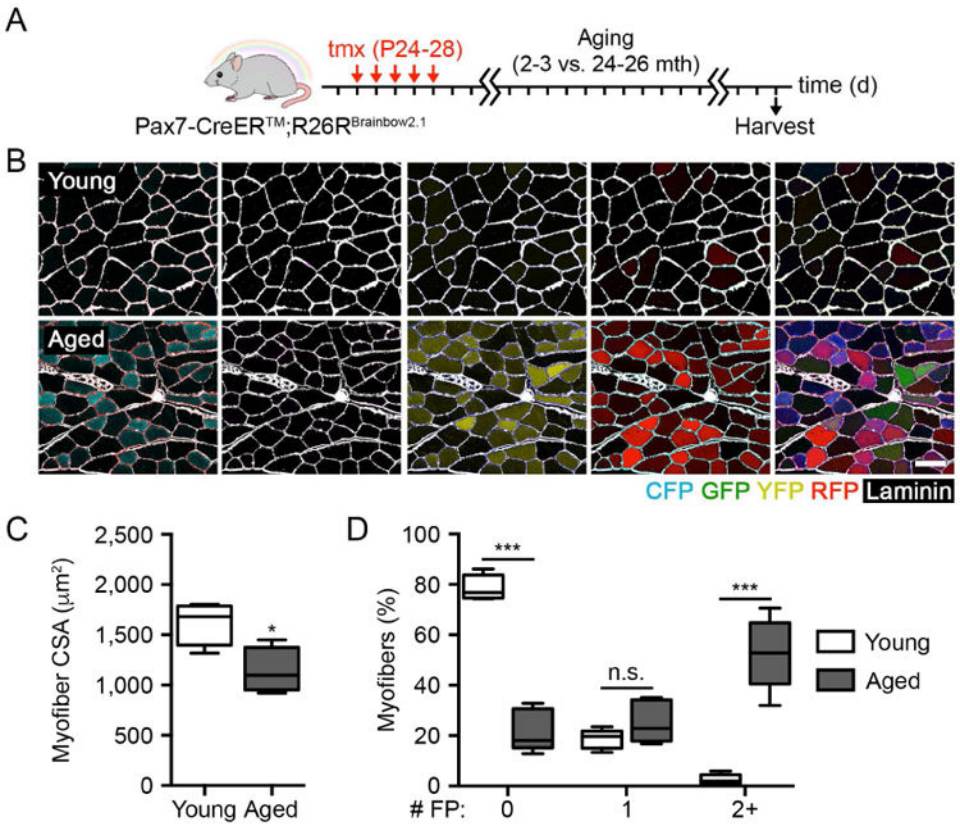

Figure 1. MuSC contribution to homeostatic aging is robust and polyclonal

(**A-B**) Scheme and identification of FP^+ myofibers in composite images following MuSC labeling and long-term lineage tracing in Pax7-CreER™; $R26R^{Brainbow2.1}$ muscles with age. Scale bar, 50 μm.

(**C-D**) Quantification of myofiber CSA and the percentage of myofibers expressing 0, 1, or 2 or more FPs in young and aged muscles (n = 5).

Data are represented as average ± SEM (***P < 0.001, *P < 0.05). See also Figure S1.

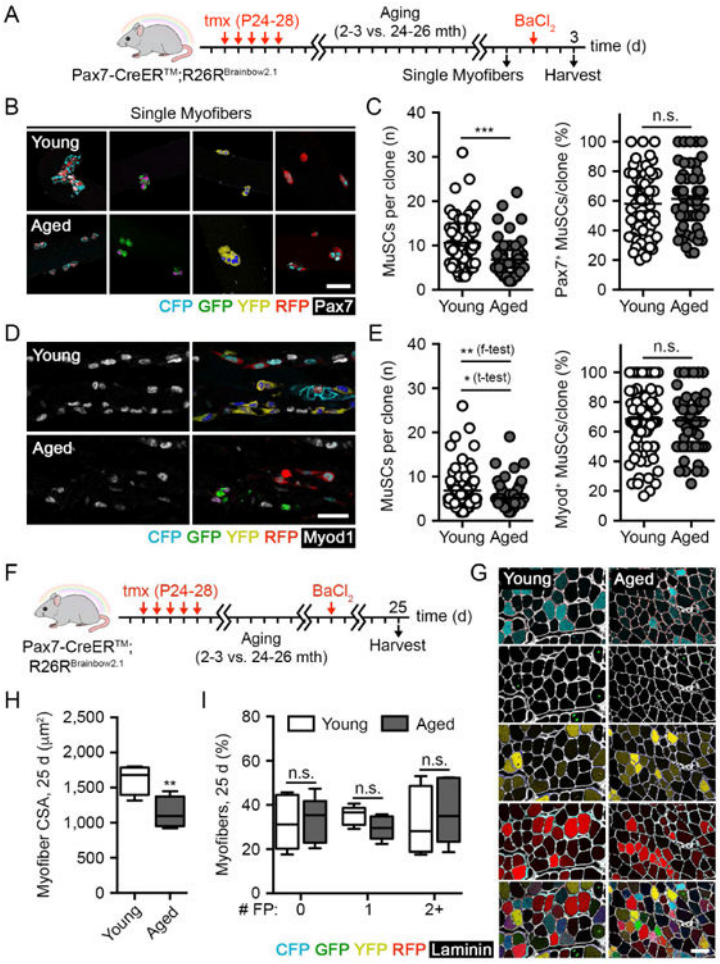

Figure 2. Functional MuSC heterogeneity, but not clonal complexity, is reduced with age

(**A**) Scheme FP^+ MuSC-derived clonal labeling in young and aged muscles upon single myofibers cultured in suspension and 3 d post-$BaCl_2$ injury.

(**B-C**) Images and quantification of FP^+ myofiber-associated MuSC clone size and the percentage of $Pax7^+$ cells per clone isolated from young and aged muscles after 3 d in suspension culture. Scale bar, 50 μm (n = 53-64 clones).

(**D-E**) Composite images and quantification of FP^+ MuSC-derived clone size and the percentage of $Myod^+$ cells per clone in young and aged muscles 3 d post-$BaCl_2$ injury. Scale bar, 50 μm (n = 62-81 clones).

(**F-G**) Scheme and identification of FP^+ myofibers in composite images of young and aged muscles 25 d post-$BaCl_2$ injury. Scale bar, 50 μm.

(**H-I**) Quantification of myofiber CSA and the percentage of myofibers expressing any number of FPs in young and aged muscles 25 d post-$BaCl_2$ injury (n = 5).

Data are represented as average ± SEM (***P < 0.001, **P < 0.01, *P < 0.05; student's t-test unless otherwise indicated). See also Figure S2.

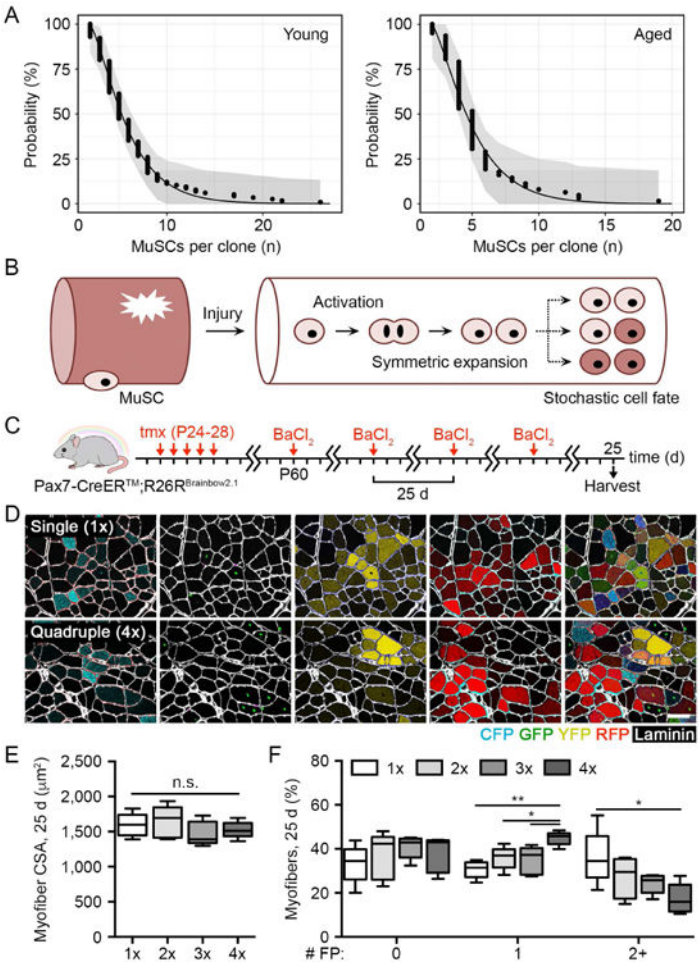

Figure 3. Symmetric expansion and stochastic fate acquisition precedes a decline in MuSC clonal complexity under constant regenerative pressure

(**A**) Young and aged MuSC cumulative clone size distributions and model predictions 3 d post-$BaCl_2$ injury. Shaded area denotes 95% Kolmogorov-Smirnov confidence intervals of empirical distribution.

(**B**) Scheme depicting young and aged MuSC behavior during the early regenerative phase.

(**C-D**) Scheme and identification of FP^+ myofibers in composite images of young muscles following serial $BaCl_2$ injury. Scale bar, 50 μm.

(**E-F**) Quantification of myofiber CSA and the percentage of myofibers expressing any number of FPs in young muscles following serial $BaCl_2$ injury (n = 5).

Data are represented as average ± SEM (**P < 0.01, *P < 0.05). See also Figure S3.

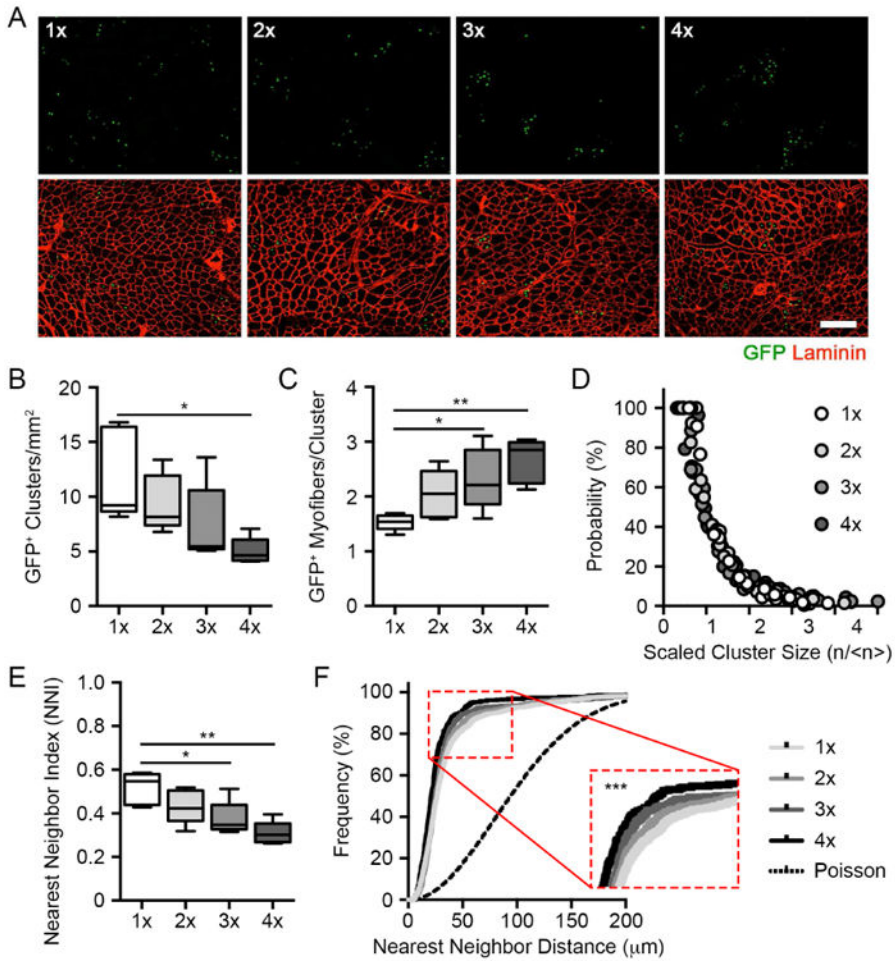

Figure 4. MuSCs follow a model of population asymmetry and neutral drift with repeated injury

(**A**) Composite images of GFP^+ myonuclei in regenerated muscles following serial $BaCl_2$ injury. Scale bar, 100 μm.

(**B-C**) Quantification of GFP^+ myofiber cluster density and the number of regenerated myofibers per cluster following serial $BaCl_2$ injury (n = 5).

(**D**) Cumulative, scaled cluster size distribution following serial $BaCl_2$ injury (199-446 clusters).

(**E-F**) Quantification of nearest neighbor index and cumulative distribution frequency derived from spatial analyses of GFP^+ nuclei following serial $BaCl_2$ injury (n = 5).

Data are represented as average ± SEM (***P < 0.001, **P < 0.01, *P < 0.05). See also Figure S4.

Key Resources Table

Reagent or resource	Source	Identifier
Animal Models		
Mouse Pax7-CreER	(Nishijo et al., 2009)	N/A
Mouse Gt(ROSA)26Sortm1(CAG-Brainbow2.1)Cle/J	Jackson Laboratories	Cat #013731
Antibodies		
Rabbit anti-Laminin	Sigma	Cat #L9393
Mouse anti-Pax7	Developmental Studies Hybridoma Bank	http://dshb.biology.uiowa.edu/PAX7
Mouse anti-Myod	Santa Cruz	Cat #sc760
Chemicals, Peptides, and Recombinant Proteins		
Tamoxifen	Sigma	Cat #T5648
Barium chloride	Sigma	Cat #202738
Software and algorithms		
ImageJ software		https://imagej.nih.gov/ij/download.html
FlowJo software		http://www.flowjo.com
Graphpad – Prism software		http://www.graphpad.com